Magnetic-dipole wavelength measurements in the $n=3$ configurations of highly ionized Cu, Zn, Ga, As, Kr, and Y

J. R. Roberts, T. L. Pittman, J. Sugar, and V. Kaufman
Atomic and Plasma Radiation Division, National Bureau of Standards, Gaithersburg, Maryland 20899

W. L. Rowan
Fusion Research Center, The University of Texas at Austin, Austin, Texas 78712
(Received 9 October 1986)

Magnetic dipole ($M1$) transitions between the levels of the ground configurations in the $3s^23p^x$ Al-like through Cl-like and the $3s\,3p$ Mg-like isoelectronic sequences of Cu, Zn, Ga, As, Kr, and Y have been observed. These elements were introduced into the Texas experimental Tokomak plasma by laser ablation of metallic thin films and gas puffing. The spectral lines were recorded by using three monochromators with photoelectric detection and a spectrometer with a channel electron multiplier array detector. Twenty-eight newly observed $M1$ lines were measured and classified.

I. INTRODUCTION

Magnetic dipole transitions in highly ionized atoms provide a means of probing high-temperature, low-density plasmas. Some lines occur at long wavelengths which are convenient for observations. They have provided noninterfering probes for ion-temperature measurements,[1] excitation-rate measurements,[2] and plasma-rotation and impurity-transport studies in tokamaks.[3]

We report in this paper the measured wavelengths of magnetic dipole ($M1$) spectral lines between levels of the ground configurations in the $3s^23p^x$ $_{13}$Al-like through $_{17}$Cl-like and the $3s\,3p$ $_{12}$Mg-like isoelectronic sequences of $_{29}$Cu, $_{30}$Zn, $_{31}$Ga, $_{33}$As, $_{36}$Kr, and $_{39}$Y. These lines were emitted by impurity atoms injected into the plasma of the Texas Experimental Tokamak (TEXT). Gas impurities were puffed into the plasma by means of a piezoelectric valve, and metallic impurities were introduced by the laser ablation technique.[4] The impurities were injected when the plasma had reached steady-state conditions. Previous measurements[5–7] in these isoelectronic sequences were the basis for semiempirical calculations of these wavelengths.[8] The present observations provide additional data which may be useful in improving the predicted wavelengths for these sequences. The combined use of an expanded experimental data base and extensive calculated predictions will allow expansion into other related sequences and higher ion stages.

II. EXPERIMENTAL ARRANGEMENT AND METHOD

TEXT (Ref. 9) generates a toroidal plasma of 27-cm minor radius and 100-cm major radius. For the experiments performed for this paper the plasma conditions were: central electron temperature of 1 keV, central line-averaged electron density of 3×10^{13} cm^{-3}, plasma current of 350 kA, and steady-state conditions for 200 ms out of a plasma duration of over 500 ms.

The tokamak and the arrangement of the apparatus are shown in Fig. 1. The experimental apparatus consisted of four spectrometers, three having photoelectric detection and one utilizing a channel electron multiplier array (CEMA) detector similar to that of Ref. 10. All were aligned to observe the toroidal plasma radially along its major radius at different positions. The wavelengths below 500 Å were observed with a 2.2-m grazing-incidence vacuum monochromator. The spectra from 700 to 2000 Å were observed with a 1-m normal incidence vacuum monochromator with a 600 line/mm grating blazed at 1500 Å and with a reciprocal linear dispersion of 16.6 Å/mm. The instrument with the CEMA was also a 1-m normal incidence vacuum spectrometer with a 1200 line/mm grating blazed at 1500 Å with a reciprocal linear dispersion of 8.3 Å/mm. The spectrometer used for wavelengths above 2000 Å was an air-path 1-m Czerny-Turner monochromator with a grating of 1200 line/mm blazed at 3000 Å. The reciprocal linear dispersion of this instrument is also 8.3 Å/mm.

The method of measuring the unknown wavelengths was as follows: The 1-m normal incidence (NI) and the 1-m Czerny-Turner (C-T) monochromators were scanned from shot to shot in wavelength increments smaller than the instrumental bandwidth. For example, if the slit width on the C-T monochromator was 100 μm, the instrumental bandwidth was 0.8 Å, and the scan increment was 0.5 Å. The signals from at least five separate wavelength points were measured for a given line profile. Each point was measured twice to give some statistics for fitting. The signals at each wavelength setting were normalized as stated below. The normalized points were fit by least squares to a Gaussian profile to determine the central wavelength and its uncertainty.

The NI instrument was calibrated from approximately 700 to 2200 Å using known lines emitted from the plasma. The uncertainties associated with this calibration were deduced the same way as for the unknown lines. The C-T instrument was wavelength calibrated using a low-pressure Hg discharge lamp above 2000 Å. The $M1$ lines measured with the NI monochromator using the

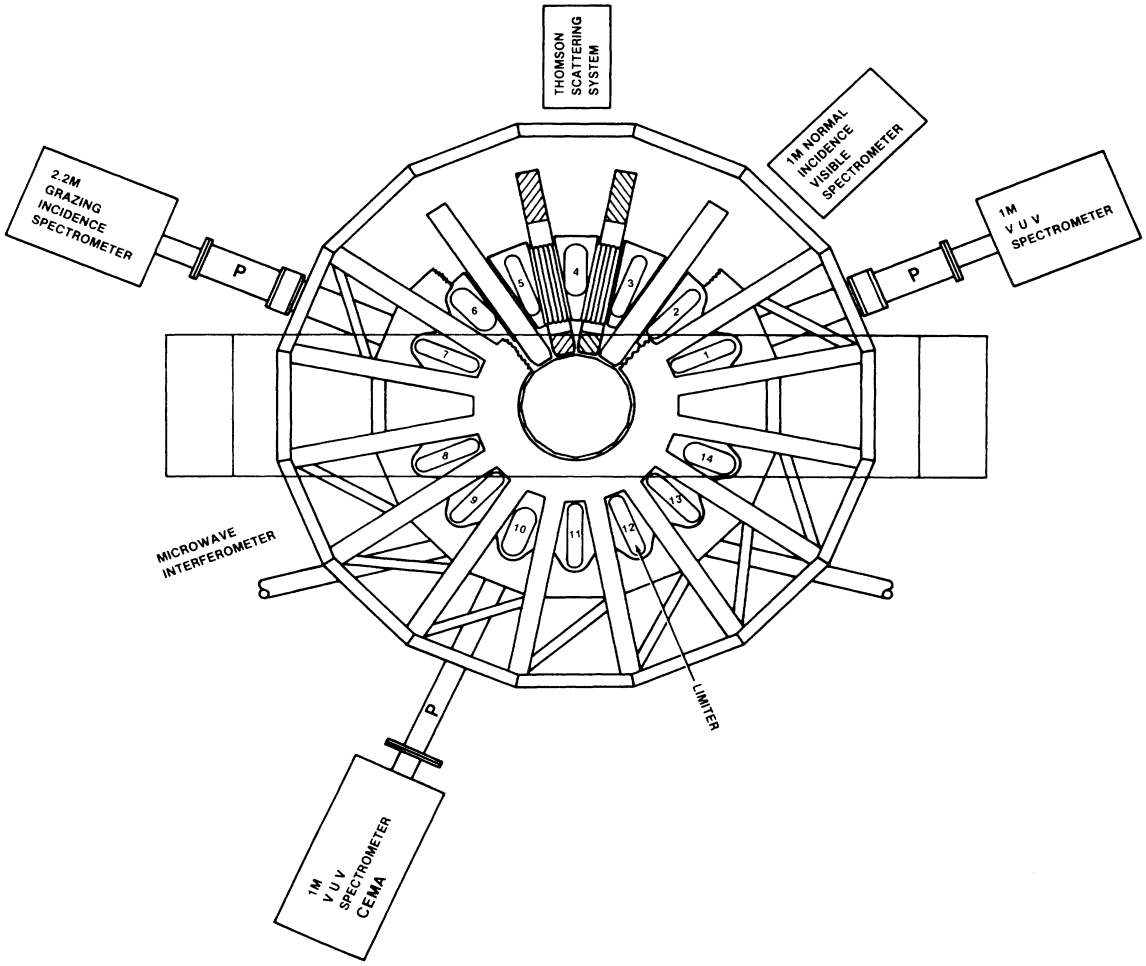

FIG. 1. Experimental arrangement of spectrometers on TEXT.

CEMA detector were calibrated with respect to nearby known lines of Fe, O, etc., recorded at the same time the $M1$ lines were observed. The uncertainty of these calibrations was convoluted with the measurement uncertainty to give a total uncertainty of the measured wavelengths. The total uncertainty varies due to ratio of the signal to background. The uncertainties of the known wavelengths used in the calibration were substantially smaller than the measured uncertainties.

The spectrometer with the CEMA was used primarily as a survey detector. Its total spectral bandpass was approximately 70 Å. It was used to verify the wavelength identifications obtained from the shot-to-shot scanning monochromators. It also indicated whether or not other lines were too close to the line in question, thus making an identification ambiguous. The spatial resolution of the CEMA system, including the CEMA and the charged-coupled-device (CCD) readout was 175 μm. This corresponded to a spectral line bandwidth of 1.45 Å. Therefore the resolution of the measurements with this detector was approximately as good as with the photoelectric detection. There were a few occasions when it was the only detector to make the observation because it integrated over a much longer time than the photomultipliers, and could thus record weaker lines. These occurrences are listed in Tables I and II by footnotes.

The elements investigated were $_{29}$Cu, $_{30}$Zn, $_{31}$Ga, $_{33}$As, $_{36}$Kr, and $_{39}$Y. The metals were injected into the plasma by laser ablation of a thin film. A 50-mm square glass plate, with a 0.1-μm film of chromium deposited onto it, was overcoated with a 2-μm thickness of the metal. The slide was placed in an evacuated chamber with the thin films toward the plasma and away from the impinging laser beam. A 2J ruby laser beam was directed onto the clear side of the glass slide. The chromium film absorbed the light from the laser and the chromium and the metal sample were ablated into the plasma. Because the chromium was the first absorbing material with which the laser beam interacted, the amount of ablated material was independent of the element to be introduced. The laser was focused to ablate a few millimeter diameter sample. The laser beam was then automatically moved to illuminate a new spot on the film. In this manner a single coated slide produced up to 100 targets for injection. The Ga and As were injected using a GaAs thin film. The injection occurred at a time when the plasma had reached a steady-

state temperature and density, approximately 250 ms after the initiation of the 500-ms-long discharge. The injected material was quickly distributed throughout the toroidal plasma and spectra from highly ionized atoms could be observed around the entire plasma within 5 ms of injection. The ablated chromium was not observed because the small quantity on the slide did not contribute to the signal ($S/N \approx 20{:}1$).

Krypton was introduced through a piezoelectric gas puff valve. The duration of its opening (usually 2 ms) and the applied voltage to the valve governed the amount of gas injected into the existing plasma. These variables were adjusted to avoid disrupting the plasma while achieving the maximum signal from the Kr lines. The spectra of highly ionized Kr took up to 50 ms to reach peak intensity.

The ion concentration varied from shot to shot because of fluctuations in the plasma conditions and film thickness; thus for averaging several shots it was necessary to monitor the density of the highly ionized species under investigation. To accomplish this the 2.2-m grazing-incidence monochromator (GI) was fixed on the wavelength of a known electric dipole line emitted by the species under investigation in the same or nearby state. This monitoring provided a normalizing signal for shot-to-shot fluctuations in the ion density and a temporally resolved signal to compare with the unknown line observed by one of the other monochromators. The temporal monitoring verified that the line under investigation was of the same or nearby ion stage, since the temporal evolution of the ion depends on the ion stage. In the case of the CEMA observations, this temporal monitoring was

TABLE I. Magnetic dipole lines observed in this experiment and compared with predictions. All wavelengths are in angstroms; those above 2000 Å are air wavelengths.

Ion	Classification	λ_{pred}	λ_{obs}	$\Delta\lambda$	λ_{unc}
	$_{17}$Cl-like				
$_{30}$Zn XIV	$^2P_{3/2}$-$^2P_{1/2}$	2922.5	2923.6	−1.1	1.0
$_{39}$Y XXIII	$^2P_{3/2}$-$^2P_{1/2}$	768.8	769.1	−0.3	0.4
	$_{16}$S-like				
$_{29}$Cu XIV	$^3P_1$-$^1S_0$	1191.0	1190.4	+0.6	0.5
$_{39}$Y XXIV	$^3P_1$-$^1D_2$	2565.0	2543.1	+21.9	0.3
$_{29}$Cu XIV	$^3P_2$-$^3P_1$	4181.0	4183.4	−2.4	0.3
$_{30}$Zn XV	$^3P_2$-$^3P_1$	3449.0	3451.4	−2.4	0.4
$_{33}$As XVIII	$^3P_2$-$^3P_1$	2030.0	2032.6	−2.6	0.3
$_{36}$Kr XXI	$^3P_2$-$^3P_1$	1269.0	1268.7	+0.3	0.2
$_{39}$Y XXIV	$^3P_2$-$^3P_1$	833.0	833.1	−0.1	0.2
$_{39}$Y XXIV	$^3P_0$-$^3P_1$	1576.0	1572.9	+3.1	1.0
	$_{15}$P-like				
$_{31}$Ga XVII	$^2D_{3/2}$-$^2P_{3/2}$	1319.0	1319.1	−0.1	0.3
$_{33}$As XIX	$^2D_{5/2}$-$^2P_{3/2}$	1294.0	1292.4	+1.6	0.2
$_{36}$Kr XXII	$^2D_{5/2}$-$^2P_{3/2}$	912.0	912.0[a]	0.0	1.0
$_{39}$Y XXV	$^4S_{3/2}$-$^2D_{3/2}$	919.0	914.7	+4.3	1.0
$_{39}$Y XXV	$^2D_{3/2}$-$^2D_{5/2}$	2700.0	2717.8	−17.8	0.3
	$_{14}$Si-like				
$_{29}$Cu XVI	$^3P_1$-$^1D_2$	1874.0	1871.3	+2.7	0.2
$_{30}$Zn XVII	$^3P_1$-$^1D_2$	1680.0	1676.9	+3.1	0.2
$_{33}$As XX	$^3P_1$-$^1D_2$	1199.0	1195.3	+3.7	0.2
$_{36}$Kr XXIII	$^3P_1$-$^1D_2$	854.0	853.8	+0.2	1.0
$_{30}$Zn XVII	$^3P_0$-$^3P_1$	4365.0	4355.0	+10.0	0.3
$_{33}$As XX	$^3P_0$-$^3P_1$	2440.0	2438.0	+2.0	0.3
$_{36}$Kr XXIII	$^3P_0$-$^3P_1$	1462.0	1461.8	+0.2	0.2
$_{39}$Y XXVI	$^3P_0$-$^3P_1$	929.0	927.7	+1.3	0.3
$_{36}$Kr XXIII	$^3P_1$-$^3P_2$	3832.0	3840.9	−8.9	0.3
$_{39}$Y XXVI	$^3P_1$-$^3P_2$	3250.0	3254.8	−4.8	1.0
	$_{13}$Al-like				
$_{30}$Zn XVIII	$^2P_{1/2}$-$^2P_{3/2}$	2531.5	2532.5	−1.0	0.3
$_{39}$Y XXVII	$^2P_{1/2}$-$^2P_{3/2}$	697.9	698.3	−0.4	0.2
	$_{12}$Mg-like				
$_{36}$Kr XXV	$^3P_1$-$^3P_2$	1277.0	1277.1	−0.1	1.0

[a]Observed with CEMA only.

not possible because the spectra could be digitally recorded only once each second.

III. RESULTS

Table I contains the experimentally determined wavelengths for the $M1$ lines. The first column gives the ion stage, the second the classification of the transition, and the third the predicted wavelength.[8,11] The fourth column gives the wavelength as determined in this experiment. The fifth column is the difference in the predicted and observed wavelengths. The sixth column contains the experimental uncertainty as determined from the goodness of fit analysis convoluted with the instrument calibration.

Some of the lines that were identified deviated substantially from their predicted wavelengths. An example of this is the $_{39}$Y line at 2543.1 Å which was found +21.9 Å from the prediction. In this case the isoelectronic sequence plot including $_{42}$Mo, $_{40}$Zr, $_{34}$Se, and $_{32}$Ge (see Ref. 11) shows the 2543.1-Å line fits the systematic trend of deviations from the predicted values in this sequence. This is an essential confirmation of the identification of this $_{39}$Y XXIV line. The 2717.8-Å $_{39}$Y XXV and the 4355.0-Å $_{30}$Zn XVII lines are also examples of this systematic trend identification procedure. In all acceptable identifications the line temporal evolution corresponded with that of the monitor.

Table II contains six lines which were only tentatively classified. The reason for the tentative identification can be seen by referring to Fig. 2. Here the wavelength difference between the measurements and the semiempirical calculations for the $_{17}$Cl-like $^2P_{3/2}$-$^2P_{1/2}$ isoelectronic sequence is plotted for elements $_{29}$Cu through $_{42}$Mo. The key to the references is the same as the compilation of Ref. 11 and are as follows: BGBR is Ref. 3 and DHSC is Ref. 5. The points identified with an "×" are from this experiment. The dashed line represents the estimated uncertainty in the semiempirical calculations. Each point is identified with its own published experimental uncertainty bars. As can be seen from this plot, two of our measurements ($_{30}$Zn and $_{39}$Y) lie within the calculated uncertainties and three do not ($_{31}$Ga, $_{33}$As, and $_{36}$Kr). Those outside do not appear to fit the systematic trend represented in this graph. However, they were the only lines within a wavelength band equal to twice the calculated uncertainty. Thus they are only tentatively identified as belonging to this isoelectronic sequence. As yet unidentified strong lines belonging to the same or other highly ionized ions of the same species may account for these lines. These lines are included in Table II for the sake of completeness of our experimental observations. Detailed analysis of their temporal evolution has not been done, but observations indicate these lines are indeed from a high ion stage near to that of the monitor ion stage.

Further investigations of the 1608.8-Å $_{33}$As XX line of Ref. 7 showed three additional highly ionized $_{33}$As or $_{31}$Ga (since GaAs is used) lines at 1600.9, 1603.9, and 1605.3 Å. This makes the identification of the $_{33}$As XX 1608.8-Å line in Ref. 7 only tentative. Similarly in Kr, additional lines appear at 868.4 and 870.6 Å also making the previous identification in Ref. 7 of the $_{36}$Kr XXI line at 877.6 Å only tentative.

An example of how the isoelectronic sequence plots of the wavelength difference between the semiempirical and measured values led to an identification from a systematic trend is depicted in Fig. 3. Here our $_{33}$As, $_{36}$Kr, and $_{39}$Y observations compare well with the calculated and other experimental values. The previously measured lines of $_{34}$Se, $_{32}$Ge, and $_{29}$Cu (Ref. 5) indicate a systematic deviation with respect to the calculations for this sequence. Our $_{33}$As and $_{30}$Zn observations conform with this trend and can be identified even though the measurements differ substantially from the calculations but are well within the calculated uncertainties. This demonstrates the advantage of having calculated predictions combined with extensive measurements.

The spectrometers used were not radiometrically calibrated, thus no indication of line intensity was given. An indication of spectral intensities can be gotten from the values of the calculated transition probabilities in Ref. 8.

IV. CONCLUSIONS

Comparison of our measurements with semiempirical calculations and other experiments indicate good agreement. Some of these data show systematic deviations which will guide further revisions of semiempirical calculations and point out where further measurements may be needed. The combination of experimental determination and semiempirical calculations of wavelengths will allow further expansions into new isoelectronic sequences and more highly ionized species, required for diagnostics of higher temperature plasmas.

TABLE II. Tentatively identified magnetic dipole lines observed in this experiment and compared with predictions. All wavelengths are in angstroms; those above 2000 Å are air wavelengths.

Ion	Classification	λ_{pred}	λ_{obs}	$\Delta\lambda$	λ_{unc}
$_{31}$Ga XV	$^2P_{3/2}$-$^2P_{1/2}$	2459.7	2456.4	+3.3	0.3
$_{33}$As XVII	$^2P_{3/2}$-$^2P_{1/2}$	1779.8	1777.2	+2.6	0.3
$_{30}$Zn XV	$^3P_2$-$^1D_2$	1706.0[a]	1702.8	+3.2	0.2
$_{33}$As XIX	$^4S_{3/2}$-$^2D_{3/2}$	1688.0	1660.4	+7.6	0.2
$_{31}$Ga XVIII	$^3P_1$-$^1D_2$	1503.0	1503.7[b]	−0.7	0.3
$_{36}$Kr XX	$^2P_{3/2}$-$^2P_{1/2}$	1144.7	1142.5	+2.2	0.2

[a]1701.4(±1.5) Å from Ref. 12.

[b]Observed with CEMA only.

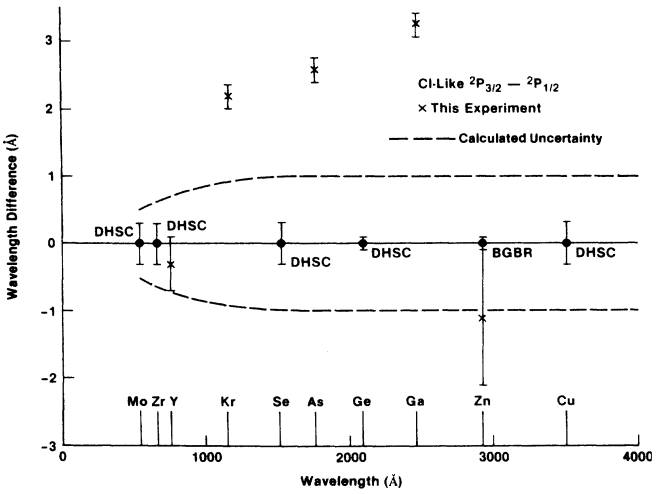

FIG. 2. The wavelength differences between observed and calculated $M1$ lines for the $_{17}$Cl-like $^2P_{3/2}$-$^2P_{1/2}$ isoelectronic sequence vs observed wavelength. The symbols represent the following: BGBR is Ref. 3., DHSC is Ref. 5, the points with an × are from this experiment, and the dashed line represents the uncertainty associated with the calculations. The points are identified by their chemical symbols.

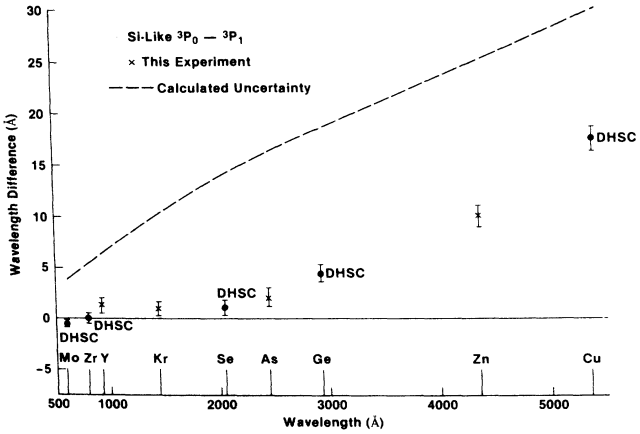

FIG. 3. The wavelength differences between observed and calculated $M1$ lines for the $_{34}$Si-like $^3P_0$-$^3P_1$ isoelectronic sequence vs observed wavelength. The symbols represent the following: BGBR is Ref. 3., DHSC is Ref. 5, the points with a × are from this experiment, and the dashed line represents the uncertainty associated with the calculations. The points are identified by their chemical symbols.

ACKNOWLEDGMENTS

The support of the TEXT staff, especially K. W. Gentle, B. Mixon, D. M. Patterson, and B. Richards is greatly appreciated. We also express our appreciation for the help given by M. Bassin, K. Leung, and C. Klepper. This work is supported by the U.S. Department of Energy under Contract Nos. EA-77-A-01-6010 and DE-AC05-78ET53043.

[1]S. Suckewer and E. Hinnov, Phys. Rev. Lett. **41**, 756 (1978).
[2]R. U. Datla, J. R. Roberts, W. L. Rowan, and J. B. Mann, Phys. Rev. A **34**, 4751 (1986).
[3]K. H. Burrell, R. J. Groebner, N. H. Brooks, and L. Rottler, Phys. Rev. A **29**, 1343 (1984).
[4]D. R. Terry, W. L. Rowan, W. J. Connally, and W. K. Leung, in Proceedings of the Tenth Symposium on Fusion Energy, Philadelphia, 1983 (unpublished).
[5]B. Denne, E. Hinnov, S. Suckewer, and S. Cohen, Phys. Rev. A **28**, 206 (1983).
[6]B. Denne, E. Hinnov, S. Suckewer, and J. Timberlake, J. Opt. Soc. Am. B **1**, 296 (1984).
[7]J. R. Roberts, V. Kaufman, J. Suger, T. L. Pittman, and W. L. Rowan, Phys. Rev. A **27**, 1721 (1983).
[8]J. Sugar and V. Kaufman, J. Opt. Soc. Am. B **1**, 218 (1984).
[9]K. W. Gentle, Nucl. Technol./Fusion **1**, 479 (1981).
[10]C. L. Cromer, J. M. Bridges, J. R. Roberts, and T. B. Lucatorto, Appl. Opt. **24**, 2996 (1985).
[11]V. Kaufman and J. Sugar, J. Phys. Chem. Ref. Data **15**, 321 (1986).
[12]J. Sugar and V. Kaufman, Phys. Scr. (to be published).